Forum geografic. Studii și cercetări de geografie și protecția mediului
Volume **XIX**, Issue **2** (**December** 2020), pp. **165-174**
http://dx.doi.org/**10.5775/fg.2020.062.d**

Flood Mapping and Estimation of Flood Water-Level Using Fuzzy Method and Remote Sensing Imagery (Case Study: Golestan Province, Iran)

Amin Jalilzadeh[1], Saeed Behzadi[1*]

[1] Department of Surveying Engineering, Faculty of Civil Engineering, Shahid Rajaee Teacher Training University, Tehran, Iran
* *Corresponding author:* behzadi.saeed@gmail.com

Received on 21.02.2020, reviewed on 01.07.2020, accepted on 27.09.2020

Abstract

Recently, the heavy precipitation occurred across the north of Iran caused an unprecedented flood. Due to the topographic conditions of the study area, not paying attention to the regular dredging of the river has caused a lot of problems for the local people. On the other hand, due to the frequent rainfall, the occurrence of flooding for a long time was another major problem. The combination of Remote Sensing and GIS can make a substantial contribution to flood assessment and management. In the present study, a fuzzy method is developed to show the hidden potential of Landsat satellite images for flood mapping. This paper presents the process of rapid access to water level information, which can provide valuable data for decision makers. The overall accuracy obtained for the flooded and damaged area is 87.23% and 46% respectively, and Root Mean Square Error (RMSE) of 27.68 cm is obtained for water-level based in the proposed algorithm.

Keywords: *GIS, water-level, flood mapping, Fuzzy, Landsat*

Rezumat. Cartografierea inundațiilor și estimarea nivelului apei în cadrul acestora utilizând teledetecția și metoda Fuzzy (Studiu de caz: provincia Golestan, Iran)

Recent, precipitațiile abundente din nordul Iranului au provocat o inundație fără precedent. Datorită condițiilor topografice din zona de studiu, neacordarea atenției la dragarea regulată a râului a cauzat o mulțime de probleme pentru localnici. Pe de altă parte, din cauza precipitațiilor frecvente, apariția inundațiilor pentru o lungă perioadă de timp a reprezentat o altă problemă majoră. Combinația dintre teledetecție și SIG poate aduce o contribuție substanțială la evaluarea și gestionarea inundațiilor. Studiul de față prezintă o metodă fuzzy pentru a arăta potențialul ascuns al imaginilor din satelit Landsat pentru cartografierea inundațiilor. SE evidențiază accesul rapid la informațiile privind nivelul apei, care poate oferi date valoroase pentru factorii de decizie. Precizia generală obținută pentru zona inundată și deteriorată este de 87,23% și respectiv 46%, iar eroarea pătrată medie a rădăcinii (RMSE) de 27,68 cm este obținută pentru nivelul apei pe baza algoritmului propus.

Cuvinte-cheie: *SIG, nivelul apei, cartografierea inundațiilor, Fuzzy, Landsat*

Introduction

Floods are one of the costliest natural disasters that have caused severe economic, social and environmental damage to humans and nature. Loss of natural vegetation and crops, animals and human life are also the other negative effect of this disaster (Haq et.al, 2012; Jeyaseelan, 2003; Pantaleoni, Engel, & Johannsen, 2007). These effects are the same in developing and advanced countries, it is therefore important that some efforts be made to manage this issue.

Large-scale heavy spring rains occurred for more than two weeks, during the first part of March 2019, throughout Iran and they had a serious impact on the lives of the people dwelling along the rivers and streams. This is one of the biggest damages caused by natural disasters in Iran in the last decade. According to the news agency near twenty-five provinces, and more than 4,400 villages were affected by floods, with 53 people dead and nearly 600 people injured. The financial damage was estimated at least 3 billion dollars. This included damage to agriculture, transportation, telecommunications, housing, and monuments. Damage to the agricultural sector is estimated at about 40% of total damage. The development of reliable and accurate models to assess economic flood impact and effective management is important for several users, such as government agencies, policymakers, researchers, insurance companies, farmers, and traders (Pantaleoni et al., 2007; Shrestha, Sawano, Ohara, Yamazaki, & Tokunaga, 2018). Providing damage estimation and adequate assistance to farmers is essential to compensate the effects of floods in risk management (Domeneghetti, Schumann, & Tarpanelli, 2019; Tapia-Silva, Itzerott, Foerster, Kuhlmann, & Kreibich, 2011).

Agriculture is the main source of income for Iranian people, which is directly affected by flood; therefore, assessing the damage caused by this type of event to the agricultural sector is definitely very

important (Behzadi, Mousavi, & Norouzi, 2019; Majumder et al., 2019; Shrestha et al., 2018). The ponding and standing water, observed in several cities after precipitation, also made people's lives difficult for a while; for example, most people had to use boats for daily commuting for several days. Consequently, understanding the water-level of the flooded area is one of the most important tasks that help people and decision-makers to manage this problem.

Since ground-based methods cannot provide an appropriate assessment of the damage for big-scale areas, the combination of Geographical Information System (GIS) and Remote Sensing (RS) can be used for flood disaster assessment (Ojo, Abegunrin, & Lasisi, 2018; Samela, Albano, Sole, & Manfreda, 2018). In addition, Digital Elevation Models (DEMs) provide a useful tool for monitoring and assessing flood disasters. (Ali & Alandjani, 2019; Brivio et.al, 2002; Haq et al., 2012; Konadu & Fosu, 2009).

Land cover maps derived from earth observation images can be used to collect an enormous amount of data even over inaccessible areas; it also provides a quick assessment for detecting the damage into agriculture sectors. This data is often available through satellite imagery (Behzadi & Memarimoghadan, 2019; Pantaleoni et al., 2007; Shrestha et al., 2018; Van der Sande, De Jong, & De Roo, 2003).

Different kinds of models have been developed by researchers to calculate the volume of the flood as well as assess its damage (Ahmed & Akter, 2017; Dutta, Herath, & Musiake, 2003; Tapia-Silva et al., 2011; Van Westen, 2013). Moreover, Ahmed and Akter (2017), Gianinetto, Villa, and Lechi (2005) and Pantaleoni et al. (2007) used the Landsat images to identify and detect flood damage in agricultural fields.

Some reviews are conducted by Huang, Chen, Zhang, and Wu (2018) and Wang and Xie (2018) to compare and analyze the existing methods. Flood modelling and prediction are the other important, and favourite topics are conducted by Demirkesen, et.al. (2007), Gianinetto et al. (2005), Konadu and Fosu (2009) and Van der Sande et al. (2003) to detect risky areas during heavy rains. Estimating the water-level is another issue that can be useful for users and decision-makers. Recently different methods have been developed and introduced for estimating water-level (Neal et al., 2009; Rakwatin et.al., 2013; Yan et.al., 2015).

According to recent studies, many existing research areas are focused on modelling and prediction of the flood to estimate the flood water-level (Kwak et.al., 2012; Tanaka et.al., 2019; Tapia-Silva et al., 2011). The performance of these methods has been proven and applicable. These methods and data are often defined based on the purpose of the model (Hiroi et.al., 2019; Jongman et al., 2012).

In this paper, four images are used to investigate the damaged vegetation lands and flooded areas. Since flood occurred in a period of time when water was accumulated in the study area, a rapid method is proposed to calculate the water level. In this method, the water level is calculated using DEM data and Landsat image. The remainder of this paper is organized as follows: in the next section, the study area and data are described. Then the proposed method is developed to calculate the volume along with the flood damage to the vegetation field. Finally, the conclusions are drawn in the last section.

Study area

Golestan province is located in the north part of Iran, in which the flood occurred from 20 March 2019 to 8 April 2019. The geographical location of the study area is 36° 51′ N to 37° 26′ N latitude, and 54° 04′ E to 54° 56′ E longitude. According to the 2011 census, the population of Golestan province is more than 1,777,000 peoples. The area of this province is 20367 square kilometres, of which more than two million hectares are under rain-fed and irrigated land. More than 50% of the cotton and 10% of the wheat of Iran are obtained from this province. About 18% and 50% of the province are covered by forests and rangelands respectively. Therefore, Golestan is an important province in terms of agriculture and forestry for Iran, which this flood caused a lot of damage to the agricultural sector.

The amount of rainfall in the Golestan province was about 300 mm in 18 and 19 March 2019, which was about 50%-70% of the annual rainfall of the area. Gonbad-e Kavus, Bandar Torkaman, Aq Qala and other cities located along the river were significantly damaged. Most of these damages were in the construction sector, urban infrastructure and especially the agricultural sector. Aq Qala was one of the first cities to attract public attention due to the severe flooding of the river. The water collected in this city had caused serious problems for the locals for nearly 30 days. Figure 1 shows the study area.

Forum geografic. Studii și cercetări de geografie și protecția mediului
Volume **XIX**, Issue **2** (**December 2020**), pp. **165-174**
http://dx.doi.org/**10.5775/fg.2020.062.d**

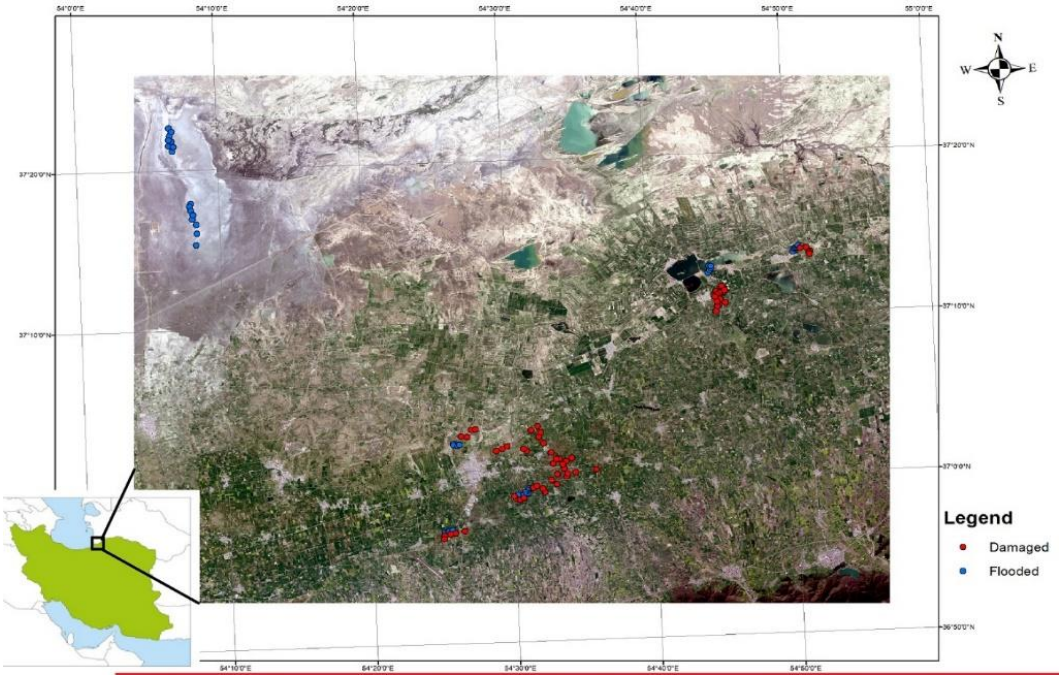

Fig. 1: Location of the Study Area

Datasets

Landsat 8 satellite images are selected as datasets; its bands are used to extract features of the area after appropriate radiometric and geometric corrections. The DEM data used in this paper is also derived from the Shuttle Radar Topography Mission (SRTM). All processing occurred at 1 arc-second (about 30-meter spatial resolution). 1 arc-second and 3 arc-second (about 90 meters) are available with worldwide coverage. The SRTM DEM used in this study has 30-meter spatial resolution. In table 1, details of Landsat 8 bands are presented.

Table 1 Landsat 8 properties

Bands	Wavelength (micrometers)	Resolution (meters)
Band 1 - coastal	0.435 - 0.451	30
Band 2 - Blue	0.452 - 0.512	30
Band 3 - Green	0.533 - 0.590	30
Band 4 - Red	0.636 - 0.673	30
Band 5 - Near Infrared (NIR)	0.851 - 0.879	30
Band 6 - Shortwave Infrared (SWIR) 1	1.566 - 1.651	30
Band 7 - Shortwave Infrared (SWIR) 2	2.107 - 2.294	30
Band 8 - Panchromatic	0.503 - 0.676	15
Band 9 - Cirrus	1.363 - 1.384	30
Band 10 - Thermal Infrared (TIRS) 1	10.60 - 11.19	100 * (30)
Band 11 - Thermal Infrared (TIRS) 2	11.50 - 12.51	100 * (30)

In this research, four Landsat 8 images are used to assess the flood damage. The first and the second images are acquired in about the same month and one year before the flood in 2018/03/15 and 2018/05/02 respectively. The third image is acquired in 2019/03/02 exactly before the flood, and the fourth image is acquired after a flood in 2019/04/03 (Table 2).

Table 2 Images used

Image	Type	Acquired date	Spatial resolution	Size of study area
1	Landsat8	2018/03/15	30mx30 m	4803.9264 km²
2	Landsat8	2018/05/02		
3	Landsat8	2019/03/02		
4	Landsat8	2019/04/03		
5	SRTM	-		

There are 110 control points collected by ground observations and in-situ data which were acquired in 2019/04/03. These data are collected in two classes: 47 sample points for flooded areas, and the rest of the sample points are for damaged areas. The flooded sample points also have depth information. These points are shown in figure 1.

Methodology

The proposed methodology consists of two processing methods: Level-1 flood mapping and Level-2 volume calculation. The workflow of the proposed methodology is presented in figure 2.

Level-1. Flood Mapping

In Level-1, the flooded and damaged areas are calculated; as a result, a flood mapping is produced. This map is then used in level-2. To assess damages of the vegetation sector, it is essential to analyze and detect changes in the vegetation and water features before and after the disaster. Since flood happened in

the early spring, there are some problems for detecting flood if only two images are used. On the one hand, the before-flood image is acquired in winter, thus the vegetation is not yet grown in some areas. On the other hand, the after-flood image is in the middle of the spring, so there is a possibility to miss affected areas. Therefore, the images of the previous year can provide valuable data to analyze the flood damage.

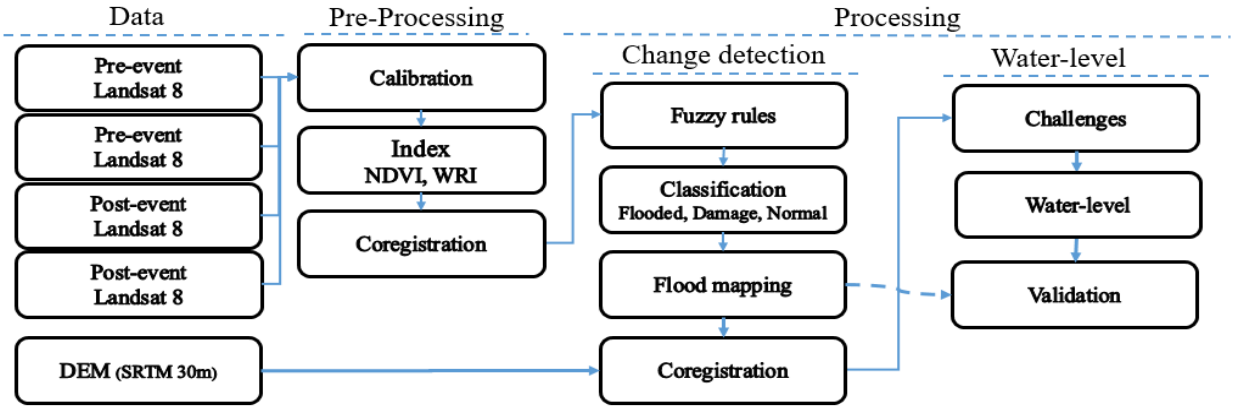

Fig. 2: General workflow

First of all, detection and classification of the target objects are needed. The features of the map are classified into three classes: Vegetation, Water, and AFEWAV (Any Feature except Water and Vegetation). Normalized Difference Vegetation Index (NDVI) (Rouse Jr, Haas, Schell, & Deering, 1974) and Water Ratio Index (WRI) (Fang-fang et al., 2011) are used to identify the dominant features of the area. NDVI quantifies vegetation, which ranges from -1 to +1. The range from 0.2 to 1 is considered as vegetation; AFEWAV features are also in the range from 0 to 0.2 (Eq.1).

$$\mathbf{NDVI} = \frac{\mathbf{NIR-Red}}{\mathbf{NIR+Red}} \qquad \text{Equation 1}$$

Finally, the WRI is used to show water area; the range bigger than 1 is considered as water in WRI (Eq.2).

$$\mathbf{WRI} = \frac{\mathbf{Green+Red}}{\mathbf{NIR+MIR}} \qquad \text{Equation 2}$$

Detecting damaged area is developed as follow: there are two pairs of images (Table 2), first pair one contains images 1 and 2, and the second pair includes images 3 and 4.

These images are used to probe the transformations behaviour of the features in these two pairs of images (before and after flood). Each pixel presents one of the features: 1- Water 2- Vegetation 3- AFEWAV.

In this step, a set of rules is specified on the set of image pairs. These rules are shown in Table 3. For example, if the pixel in the first image pair changes from AFEWAV to the Vegetation and the same process occurs in the second image pair, the pixel is considered as a normal class. Or if the pixel in the first image pair changes from Vegetation state to a state AFEWAV than Water, but in the second image pair, the same pixel changes to a Water state, this pixel is considered as a flood class.

In addition to these rules, a series of simple rules is also specified based on only one image pair (second image pair). For example, in the second image pair, if the pixel in the first image is in the Vegetation or AFEWAV type and this pixel changes to Water in the second image, this pixel belongs to the flood class. Also, if the pixel changes from the Vegetation or Water state to the AFEWAV state, this pixel belongs to the damaged class.

Table 3 Fuzzy rules for generating flood map

1.	If (NDVI1 is low) and (NDVI2 is high) and (NDVI3 is low) and (NDVI4 is high) and then (output1 is normal)
2.	If (NDVI1 is low) and (NDVI3 is low) and (WRI2 is high) and (WRI4 is high) and then (output1 is normal)
3.	If (NDVI1 is high) and (NDVI3 is high) and (WRI2 is high) and (WRI4 is high) and then (output1 is normal)
4.	If (NDVI1 is high) and (NDVI2 is low) and (NDVI3 is high) and (NDVI4 is low) and then (output1 is normal)
5.	If (NDVI2 is high) and (NDVI4 is high) and (WRI1 is high) and (WRI3 is high) and then (output1 is normal)
6.	If (NDVI2 is low) and (NDVI4 is low) and (WRI1 is high) and (WRI3 is high) and then (output1 is normal)
7.	If (NDVI1 is high) and (NDVI3 is low) and (WRI2 is not high) and (WRI4 is high) and then (output1 is Flood)
8.	If (NDVI1 is low) and (NDVI3 is low) and (WRI2 is not high) and (WRI4 is high) and then (output1 is Flood)
9.	If (NDVI1 is high) and (NDVI2 is not low) and (NDVI3 is high) and (NDVI4 is low) and then (output1 is Damaged)
10	If (NDVI2 is not low) and (NDVI4 is low) and (WRI1 is high) and (WRI3 is high) and then (output1 is Damaged)

These rules are considered as the core of the fuzzy set (table 4). A membership function is defined as $\mu(A):X \rightarrow [0,1]$ for a fuzzy set A on the universe of discourse X, which element of X is mapped to a value between 0 and 1. Membership value or degree of

Forum geografic. Studii și cercetări de geografie și protecția mediului
Volume **XIX**, Issue **2** (**December 2020**), pp. **165-174**
http://dx.doi.org/**10.5775/fg.2020.062.d**

membership quantifies the grade of membership of the element in X to the fuzzy set A. Membership functions allow us to graphically represent a fuzzy set. Different membership function such as Gaussian membership (gaussmf) Z-shaped membership (zmf) and S-shaped membership (smf) are considered for different layers in this study. The S-shaped and Z-shaped memberships work based on two degree polynomial and the Gaussian membership function works based on Gaussian function (see Nauck, Klawonn, and Kruse (1997) and Azar (2010) for more explanation).

This set of rules is considered as a fuzzy inference engine. By applying fuzzy rules on two pairs of images, the class is specified for each pixel. The sum of the pixels in each class is then calculated.

Table 4. Adopted parameters to model the fuzzy set

Layer	Sematic attribute	Fuzzy set
WRI	High	smf
NDVI	Low	zmf
NDVI	High	smf
Product	Flooded	zmf
Product	Normal	gaussmf
Product	Damaged	smf

The pixels of the flooded and damaged areas are shown in Figures 3 and 4 with different colours for the proposed and simple methods. Also, the difference between the results of the proposed and simple method is shown in Figure 5. Table 5 also shows the estimated number of pixels in the proposed and simple methods.

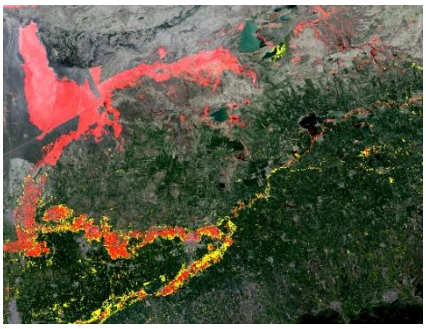

Fig. 3: Flooded (red) and damaged (yellow) pixels for Proposed method

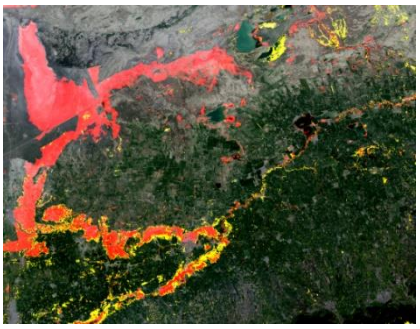

Fig. 4: Flooded (red) and damaged (yellow) pixels for Simple method

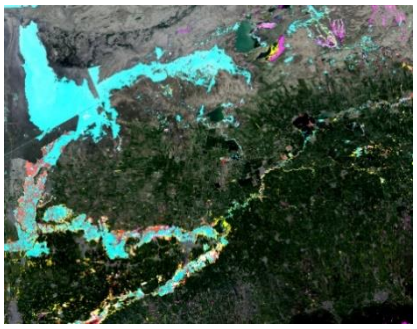

Fig. 5: Differences and similarities between the two methods based on table 6

Table 5 Pixel numbers for each class

Condition	PIXEL Numbers	Color
Proposed method		
Flooded	570744	Red
Damaged	120285	Yellow
Simple-method		
Flooded	662995	Cyan
Damaged	189623	Magenta

The condition of the pixels is then compared to these two methods. For this purpose, the pixels that exist in different classes in simple and proposed methods are counted, and their results are then compared. The results of this comparison are shown in Table 6. This table specifies the number of pixels that are in different classes in the simple and proposed methods. The colour assigned to each of these pixels is also specified in this table.

Table 6 Comparison Proposed method and simple method

	Simple	Proposed	Number pixels	color
1	Flooded	Flooded	570744	Cyan
2	Flooded	Not Flooded	92251	Red
3	Not Flooded	Flooded	0	Black
4	Damaged	Damaged	120585	Yellow
5	Damaged	Not Damaged	69338	Magenta
6	Not Damaged	Damaged	205	Blue

As seen in table 6, the simple-method covers all flooded pixels in the proposed method, and the differences in row 3 of table 6 are zero; however, 205 pixels are considered as damaged which were not damaged in simple-method obviously; this is due to the presence of vegetation that did not exist in the winter (before the flood). As seen, the simple-method detects some areas as flooded or damaged, which is normal. For example, spring rainfall can cause a rise in water level each year; these areas can be indicated as flooded areas if only two images are used; however, these areas are considered as normal areas

if more than two images are used. Moreover, the percentage of pixels that are damaged or flooded in the simple-method but they are not damaged nor flooded in the proposed method are 38% and 15%, respectively. The reason for this difference is that the simple method does not consider seasonal variation while these changes are considered in the proposed method.

Level-2. Depth and Volume calculation

In this article, we tried to develop a method for calculating the depth of each pixel after the flood. Also, the tasks of finding water-level in the proposed method are investigated. This method is not based on prediction nor simulation; it is not based on knowing the rainfall amount either. Actually, this method gives the depth of each pixel based on DEM data and flood mapping. In the proposed method, flood mapping is extracted at first. Then the SRTM map is used to detect the elevation of each pixel.

Figure 6 shows an example from the front view. There are numerous water pixels, some of which are interconnected to make an area. Generally, there are two clear rules in standing-water: First, all interconnected water pixels have one level. Secondly, every separated water-areas have different levels. Some areas have a structure as Figure 6, and the neighboring dry-pixels are suitable candidates for calculating water level. In this structure, the height of neighboring dry-pixel is always bigger than or equal to water-pixels. However, the neighboring dry-pixel is not always bigger than water-pixel in some area as seen in Figure 7. Figure 7 shows a complex surface as well as its pixelated one.

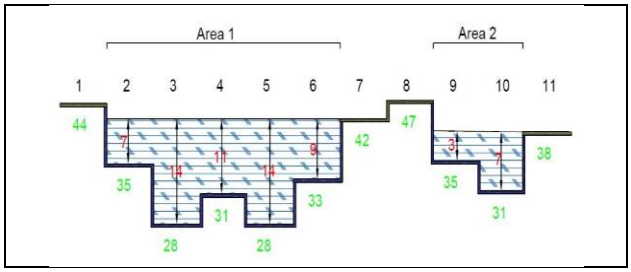

Fig. 6: A sample front view

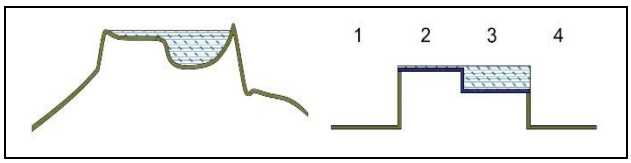

Fig. 7: Sample of a complex surface and pixelated view

Obviously, the least the value of neighboring dry-pixel is not a suitable candidate for water-level for some area (as shown in Figure 7). Therefore, Equation 3 is proposed to find the water level in the area. Based on Equation 3, if the smallest neighboring dry-pixel is smaller than the water-pixels, the greatest value of water pixels is considered as the water level in the area.

WL (a) = max (min (neighboring dry-pixels); max (water-pixels in an area)) Equation 3

Equation 3 is used to find water-level among neighboring pixels. So, in Figure 7 the pixel number 2 will be considered as water level.

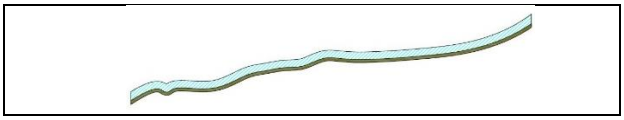

Fig. 8: A real structure

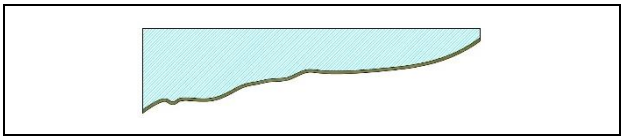

Fig. 9: An error in usual method to finding water level

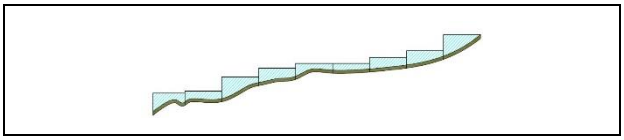

Fig. 10: A simple solution

Another problem is the flowing water area which is shown in Figure 8. If only the two simple rules mentioned for standing water are considered for running water, the running water level will be equal to its maximum height of running water, which is not logical (as shown in Figure 9). To overcome this challenge, the depth of running water needs to be calculated piecewise. In this case, the behavior of running water is shown in Figure 10, which is close to reality. Figure 11 shows the method of finding the depth of each pixel.

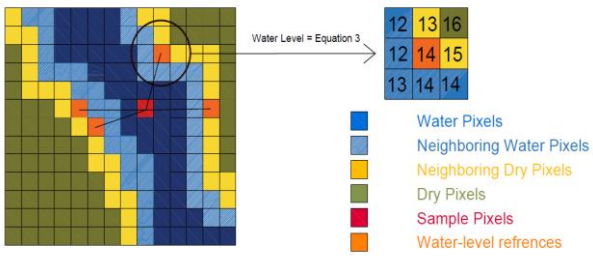

Fig. 11: Proposed method

As seen in Figure 11, the water level of each pixel is calculated based on the elevation of four near dry pixel. The value of the dry pixel is also calculated by Equation3. Now the mean of four obtained reference value is considered as the water level of sample-pixel. Since each pixel has depth information, the volume of the area is calculable. These steps are implemented for all water pixels in the study area. Figures 12 and 13 show water pixels in second pairs of images

Forum geografic. Studii și cercetări de geografie și protecția mediului
Volume **XIX**, Issue **2** (**December 2020**), pp. **165-174**
http://dx.doi.org/**10.5775/fg.2020.062.d**

(image 3 and image 4 in table 2). Extracted flood mapping through level 1 is also shown in Figure 14. The water level of each pixel is then calculated and validated.

Finally, contingency Table is used to present accuracy. Overall accuracy and Producer's accuracy of each class is calculated as:

$$\text{Overal accuracy} = \frac{\sum_{i=1}^{r} x_{ii}}{N} \qquad \text{Equation 4}$$

The overall accuracy is calculated as the total number of correctly classified pixels (diagonal elements) divided by the total number of test pixels.

$$\textbf{Producer's accuracy} = \frac{\mathbf{NC_{correctly}}}{\mathbf{NC_{ref}}} \qquad \text{Equation 5}$$

Where, $NC_{correctly}$ is the number of correctly classified pixels, and NC_{ref} *is* the number of ground reference pixels in the specified class.

Table 7 Contingency Table

Reference data / Proposed method	Flooded	Normal	Damage	Row total
Flooded	41	-	16	57
Normal	2	-	18	20
Damage	4	-	29	33
Column total	47	-	63	110

The obtained overall accuracy is near 63.46%, and the Producer's accuracy is 87.23% and 46% respectively for flooded and damaged areas. 47 sample flooded points are used to validate estimated water-level.

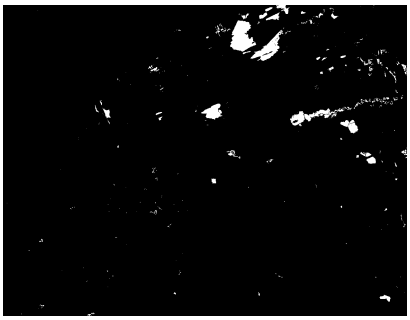

Fig. 12: Water pixels before the flood

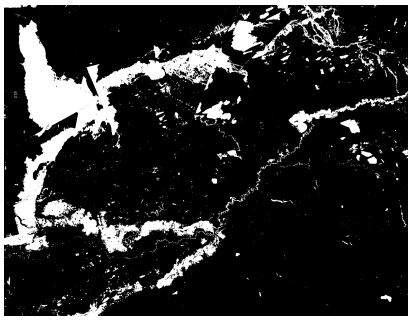

Fig. 13: Water pixels after the flood

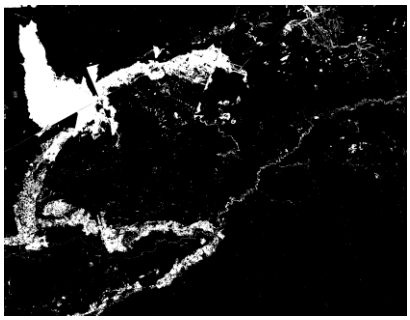

Fig. 14: Flood mapping obtained through level-1

Coefficient of determination ($\boldsymbol{R^2}$) and RMSE of estimated water-level is calculated as:

$$\boldsymbol{R^2} = \mathbf{1} - \frac{\boldsymbol{SSE}}{\boldsymbol{SST}} = \mathbf{1} - \frac{\sum_{i=1}^{n}(\boldsymbol{y_i} - \boldsymbol{O_i})^2}{\sum_{i=1}^{n}(\boldsymbol{O_i} - \boldsymbol{\mu_o})^2} \qquad \text{Equation 6}$$

$$\mathbf{RMSE} = \sqrt{\frac{1}{n}\sum_{i=1}^{n}(\mathbf{y_i} - \mathbf{O_i})^2} \qquad \text{Equation 7}$$

Where y_i is estimated values, O_i is elevation in-situ data, and μ_o is mean of the in-situ data.

In fact, $\boldsymbol{R^2}$ shows the correlation between the estimated water level height and the measured one, and RMSE measures the water level height estimation error of the measured value. These two statistical parameters evaluate the ability of the proposed model to estimate the water level height. Comparing the obtained results and actual observation shows $R^2 = 0.538$ and $RMSE = 27.68\ cm$ (Figure 15).

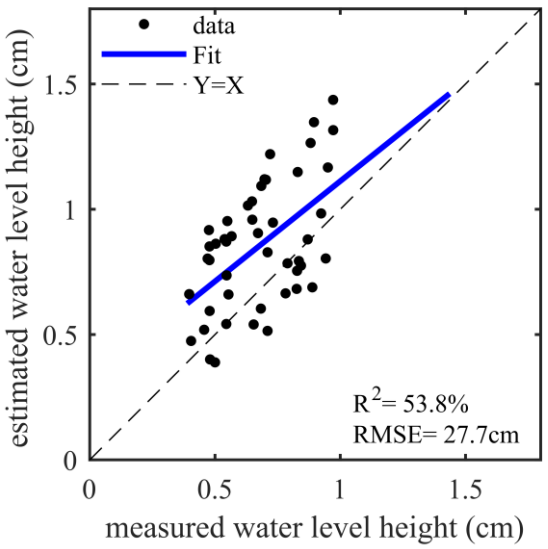

Fig. 15: The obtained results and actual observation Compilation

Discussion

The present study is divided into two phases. In the first phase, the area of flooded and damaged areas was calculated. The second phase of the study calculated the depth of water collected in the study area. In the calculation phase of flooded and damaged areas, intelligent fuzzy rules were used on the two pairs of images. The accuracy of identifying flooded and damaged areas was respectively 87% and 47%. In the second phase of the research, the accuracy of the water-level obtained, which was 27.68 cm for the flooded areas. These results show that the proposed algorithms give a rapid estimation of water-level and flood mapping for flooded areas. Despite the high accuracy for identifying flooded areas, the model was not able to identify the damaged areas well. Spring season is one of the main reasons for the low accuracy of the results to identify the damaged areas. Since the growth of some plants is not complete at the time of the flood, the proposed algorithm considers those areas as damaged. This reduces the accuracy of identifying damaged areas. This low accuracy was initially presented for flooded areas as well, but by adding two more images, these challenges were solved somewhat, and the results can confirm that. The results obtained for calculating water depth were also satisfactory. The idea of combining DEM with satellite images was the main reason of achieving this accuracy. This idea was able to reduce the error of altitude in the calculations.

Conclusion

Accurate area and depth calculation of flooded areas are one of the main concerns of decision-makers in rainy areas. Flood mapping, damage assessment, and rapid water-level calculations are crucial for conducting an effective response to mitigate the flood disaster. In this paper, an improved rapid method was introduced for flood mapping and water-level calculations based on the combination of Landsat 8, SRTM, and fuzzy sets.

The proposed method includes two levels: The first level provides an improved flood mapping method to detect flooded and damaged area by using two pairs of images. This method avoids detecting area that is routinely under the water or damaged in early spring. In level-2, a simple and rapid algorithm is developed to find the water level of the area. Finally, ground observation data was used for validation, which proved that the proposed algorithm can provide a rapid and time-consuming process to find water-level and produce flood-mapping.

The findings of the paper showed that the proposed method is an efficient, accurate and cheap (due to the free image of the landsat8 satellite), which can quickly calculate the volume and area of the flooded area. These methods can help authorities to make better decisions to assess the damage, and decrease the consequences of the flood. Although there are some other data sets such as Radar and Altimetry, which can perform better result, they may not be accessible in every area, or they may need heavy processing. Landsat 8 data, can provide timely information to assess the damage and volume of the flooded area rapidly.

However, there are some serious challenges, such as the long-time interval between images (16 days). Moreover, taken images can be cloudy, which makes the images useless. Other satellite images such as Sentinel images can be used, which are based on radar technology to overcome these challenges, then the proposed method can be applied to them to get even better results. This can be part of the future work, and even new algorithms can be developed for the calculations.

Acknowledgements

The authors thank local researchers for their help in collecting ground observations. The authors also thank the National Aeronautics and Space Administration (NASA) and the United States Geological Survey (USGS) for providing and making valuable satellite data. Moreover, the authors would like to thank the anonymous reviewers for their valuable and constructive comments on the earlier version of the manuscript.

References

Ahmed, K. R., & Akter, S. (2017). Analysis of landcover change in southwest Bengal delta due to floods by NDVI, NDWI and K-means cluster with Landsat multi-spectral surface reflectance satellite data. Remote Sensing Applications: Society Environmental monitoring assessment, 8, 168-181. doi:https://doi.org/10.1016/j.rsase.2017.08.010

Ali, S., & Alandjani, G. (2019). Mapping Land Cover Damages in Mega Floods through Integration of Remote Sensing and GIS Techniques. c Tecnología: glosas de innovación aplicadas a la pyme, 8(29), 258-275. doi:http://dx.doi.org/10.17993/3ctecno.2019.specialissue2.258–275

Azar, A. T. (2010). Fuzzy systems: BoD–Books on Demand.

Behzadi, S., & Memarimoghadan, K. (2019). A Belief-Desire-Intention Agent-based procedure for urban land growth simulation. A case study of

Tehran Metropolitan Region, Iran. Forum Geografic, 18(1), 53--62.

Behzadi, S., Mousavi, Z., & Norouzi, E. (2019). Mapping Historical Water-Supply Qanat Based On Fuzzy Method. An Application to the Isfahan Qanat (Isfahan, Iran). International Journal of Numerical Methods in Civil Engineering, 3(4), 24-32.

Brivio, P., Colombo, R., Maggi, M., & Tomasoni, R. (2002). Integration of remote sensing data and GIS for accurate mapping of flooded areas. International Journal of Remote Sensing, 23(3), 429-441. doi:https://doi.org/10.1080/01431160010014729

Demirkesen, A., Evrendilek, F., Berberoglu, S., & Kilic, S. (2007). Coastal flood risk analysis using Landsat-7 ETM+ imagery and SRTM DEM: A case study of Izmir, Turkey. Environmental monitoring assessment, 131(1-3), 293-300. doi:https://doi.org/10.1007/s10661-006-9476-2

Domeneghetti, A., Schumann, G. J.-P., & Tarpanelli, A. (2019). Preface: Remote Sensing for Flood Mapping and Monitoring of Flood Dynamics. Remote Sensing doi:https://doi.org/10.3390/rs11080943

Dutta, D., Herath, S., & Musiake, K. (2003). A mathematical model for flood loss estimation. Journal of hydrology, 277(1-2), 24-49.

Fang-fang, Z., Bing, Z., Jun-sheng, L., Qian, S., Yuanfeng, W., & Yang, S. (2011). Comparative Analysis of Automatic Water Identification Method Based on Multispectral Remote Sensing. 11, 1482-1487. doi:https://doi.org/10.1016/j.proenv.2011.12.223

Gianinetto, M., Villa, P., & Lechi, G. (2005). Postflood damage evaluation using Landsat TM and ETM+ data integrated with DEM. IEEE Transactions on Geoscience Remote Sensing, 44(1), 236-243. doi:https://doi.org/10.1109/TGRS.2005.859952

Haq, M., Akhtar, M., Muhammad, S., Paras, S., & Rahmatullah, J. (2012). Techniques of Remote Sensing and GIS for flood monitoring and damage assessment: A case study of Sindh province, Pakistan. The Egyptian Journal of Remote Sensing Space Science, 15(2), 135-141. doi:https://doi.org/10.1016/j.ejrs.2012.07.002

Hiroi, K., Murakami, D., Kurata, K., & Tashiro, T. (2019). Investigation into Feasibility of Data Assimilation Approach for Flood Level Estimation Using Temporal-Spatial State Space Model. Paper presented at the 2019 IEEE International Conference on Big Data and Smart Computing

Huang, C., Chen, Y., Zhang, S., & Wu, J. (2018). Detecting, extracting, and monitoring surface water from space using optical sensors: A review. Reviews of Geophysics, 56(2), 333-360. doi:https://doi.org/10.1029/2018RG000598

Jeyaseelan, A. (2003). Droughts & floods assessment and monitoring using remote sensing and GIS. In Satellite remote sensing and GIS applications in agricultural meteorology (Vol. 291): World Meteorol. Org. Dehra Dun, India. Geneva, Switz.

Jongman, B., Kreibich, H., Apel, H., Barredo, J., Bates, P., & Feyen, L. (2012). Comparative flood damage model assessment: towards a European approach. doi:https://doi.org/10.5194/nhess-12-3733-2012

Konadu, D., & Fosu, C. (2009). Digital elevation models and GIS for watershed modelling and flood prediction–a case study of Accra Ghana. In Appropriate Technologies for Environmental Protection in the Developing World (pp. 325-332): Springer.

Kwak, Y., Park, J., Yorozuya, A., & Fukami, K. (2012). Estimation of flood volume in Chao Phraya River basin, Thailand, from MODIS images couppled with flood inundation level. Paper presented at the 2012 IEEE International Geoscience and Remote Sensing Symposium.

Majumder, R., Bhunia, G. S., Patra, P., Mandal, A. C., Ghosh, D., & Shit, P. K. (2019). Assessment of flood hotspot at a village level using GIS-based spatial statistical techniques. Arabian Journal of Geosciences, 12(13), 409. doi:http://dx.doi.org/10.1007/s12517-019-4558-y

Nauck, D., Klawonn, F., & Kruse, R. (1997). Foundations of neuro-fuzzy systems: John Wiley & Sons, Inc.

Neal, J. C., Bates, P. D., Fewtrell, T. J., Hunter, N. M., Wilson, M. D., & Horritt, M. S. (2009). Distributed whole city water level measurements from the Carlisle 2005 urban flood event and comparison with hydraulic model simulations. Journal of hydrology, 368(1-4), 42-55. doi:https://doi.org/10.1016/j.jhydrol.2009.01.026

Ojo, O., Abegunrin, T., & Lasisi, M. (2018). Application of Remote Sensing (RS) and Geographic Information System (GIS) in Erosion Risk Mapping: Case Study of Oluyole Catchment Area, Ibadan, Nigeria. Archives of Current Research International, 1-11. doi:https://doi.org/10.9734/ACRI/2018/37585

Pantaleoni, E., Engel, B., & Johannsen, C. (2007). Identifying agricultural flood damage using Landsat imagery. Precision Agriculture, 8(1-2), 27-36. doi:https://doi.org/10.1007/s11119-006-9026-5

Rakwatin, P., Sansena, T., Marjang, N., & Rungsipanich, A. (2013). Using multi-temporal remote-sensing data to estimate 2011 flood area

and volume over Chao Phraya River basin, Thailand. Remote sensing letters, 4(3), 243-250. doi:https://doi.org/10.1080/2150704X.2012.723833

Rouse Jr, J. W., Haas, R., Schell, J., & Deering, D. (1974). Monitoring vegetation systems in the Great Plains with ERTS.

Samela, C., Albano, R., Sole, A., & Manfreda, S. (2018). A GIS tool for cost-effective delineation of flood-prone areas. Computers, Environment Urban Systems, 70, 43-52. doi:https://doi.org/10.1016/j.compenvurbsys.2018.01.013

Shrestha, B. B., Sawano, H., Ohara, M., Yamazaki, Y., & Tokunaga, Y. (2018). Methodology for Agricultural Flood Damage Assessment. In Flood Risk Management: IntechOpen.

Tanaka, K., Fujihara, Y., Hoshikawa, K., & Fujii, H. (2019). Development of a flood water level estimation method using satellite images and a digital elevation model for the Mekong floodplain. Hydrological sciences journal, 64(2), 241-253. doi:https://doi.org/10.1080/02626667.2019.1578463

Tapia-Silva, F.-O., Itzerott, S., Foerster, S., Kuhlmann, B., & Kreibich, H. (2011). Estimation of flood losses to agricultural crops using remote sensing. Physics Chemistry of the Earth, 36(7-8), 253-265. doi:https://doi.org/10.1016/j.pce.2011.03.005

Van der Sande, C., De Jong, S., & De Roo, A. (2003). A segmentation and classification approach of IKONOS-2 imagery for land cover mapping to assist flood risk and flood damage assessment. International Journal of applied earth observation geoinformation, 4(3), 217-229. doi:https://doi.org/10.1016/S0303-2434(03)00003-5

Van Westen, C. J. (2013). Remote sensing and GIS for natural hazards assessment and disaster risk management. Treatise on geomorphology, 3, 259-298. doi:https://doi.org/10.1016/B978-0-12-374739-6.00051-8

Wang, X., & Xie, H. (2018). A review on applications of remote sensing and geographic information systems (GIS) in water resources and flood risk management. In: Multidisciplinary Digital Publishing Institute.

Yan, K., Di Baldassarre, G., Solomatine, D. P., & Schumann, G. J. P. (2015). A review of low-cost space-borne data for flood modelling: topography, flood extent and water level. Hydrological processes, 29(15), 3368-3387. doi:https://doi.org/10.1002/hyp.10449.